Earth and Planetary Science Letters 485 (2018) 1–8

Contents lists available at ScienceDirect

Earth and Planetary Science Letters

www.elsevier.com/locate/epsl

Direct thermal effects of the Hadean bombardment did not limit early subsurface habitability

R.E. Grimm *, S. Marchi

Planetary Science Directorate, Southwest Research Institute, 1050 Walnut St #300, Boulder, CO, USA

ARTICLE INFO

Article history:
Received 10 July 2017
Received in revised form 5 December 2017
Accepted 22 December 2017
Available online 5 January 2018
Editor: W.B. McKinnon

Keywords:
Hadean bombardment
impact heating
thermal evolution
habitability

ABSTRACT

Intense bombardment is considered characteristic of the Hadean and early Archean eons, yet some detrital zircons indicate that near-surface water was present and thus at least intervals of clement conditions may have existed. We investigate the habitability of the top few kilometers of the subsurface by updating a prior approach to thermal evolution of the crust due to impact heating, using a revised bombardment history, a more accurate thermal model, and treatment of melt sheets from large projectiles (>100 km diameter). We find that subsurface habitable volume grows nearly continuously throughout the Hadean and early Archean (4.5–3.5 Ga) because impact heat is dissipated rapidly compared to the total duration and waning strength of the bombardment. Global sterilization was only achieved using an order of magnitude more projectiles in 1/10 the time. Melt sheets from large projectiles can completely resurface the Earth several times prior to ∼4.2 Ga but at most once since then. Even in the Hadean, melt sheets have little effect on habitability because cooling times are short compared to resurfacing intervals, allowing subsurface biospheres to be locally re-established by groundwater infiltration between major impacts. Therefore the subsurface is always habitable somewhere, and production of global steam or silicate-vapor atmospheres are the only remaining avenues to early surface sterilization by bombardment.

1. Introduction

The Hadean eon, formally defined as beginning with Earth's accretion ∼4.6 Ga and ending at 4.0 Ga (International Commission on Stratigraphy, 2017), has long been visualized as a calamitous time in Earth's history. By its original definition, no rocks were thought to be preserved from the Hadean (Cloud, 1972). Planetesimal bombardment was still relatively intense; indeed, the Hadean includes late accretion due to ongoing collisions with numerous planetary embryos >100–1000 km in diameter (e.g., Bottke et al., 2010). Impact rates decreased in the early Archean eon, although there may have been a terminal cataclysm or Late Heavy Bombardment (LHB) at ∼3.9 Ga (see Kring and Cohen, 2002, for a review). Accretional heat and radioactive heating were maximized, perhaps causing a global geodynamic style different from plate tectonics (O'Neill and Debaille, 2014). Nonetheless, some detrital zircons with Hadean crystallization ages have $^{18}O/^{16}O$ compatible with clay minerals (Mojzsis et al., 2001; Wilde et al., 2001), implying that liquid water existed near the surface of the Earth. The Hadean apparently was a time of both calamity and complexity.

The bombardment history, near-surface temperatures, and existence of water in the Hadean and early Archean are important constraints on habitability, the conditions suitable for the emergence and sustenance of life. Sleep and Zahnle (1998) performed pioneering basic calculations on the effects of impacts on early habitability. They concluded that global distribution of ejecta (including transient silicate vapor atmospheres) was the chief danger for Earth and Mars. For Earth, thermal radiation could be absorbed by ocean boiling, whereas for a dry Mars, the surface was inferred to be frequently melted (see also Abramov and Mojzsis, 2016). In contrast, Ryder (2002) argued that much of the Hadean proper was relatively peaceful since the early lunar impact flux appeared to be concentrated into the LHB, and even the LHB was insufficient to produce ocean-evaporating, globally sterilizing events. Abramov and Mojzsis (2009) and Abramov et al. (2013) performed detailed global thermal-history models due to LHB heating, including effects on habitability. They found no plausible situation in which subsurface habitable zones were fully sterilized. Marchi et al. (2014) developed a new bombardment model for the Hadean and early Archean. They refined the timing and size of impactors, including during the LHB, and also determined that projectiles with diameters >100 km can produce melt sheets that cumulatively resurface the Earth.

* Corresponding author.
E-mail address: grimm@boulder.swri.edu (R.E. Grimm).

https://doi.org/10.1016/j.epsl.2017.12.043
0012-821X/

In this paper, we reassess the influence of post-Moon-forming impacts on subsurface microbial habitability of the Earth for three reasons. First, we incorporate an updated bombardment history that has a more gradual decline and a "sawtooth" LHB instead of a spike (Marchi et al., 2014). Second, we demonstrate that the thermal model of Abramov and Mojzsis (2009) and Abramov et al. (2013) was spatially under-resolved, and we seek to determine how this may have influenced their conclusion that even a short, intense LHB would not fully sterilize the subsurface. Third, we wish to determine thermal effects and implications for habitability of emplacement of the huge melt sheets that are formed by the largest projectiles.

2. Methods

Our approach consists of five principal steps: (1) specify alternative bombardment histories (projectile diameter and time of impact, with both quantities in discrete bins or steps), (2) calculate the initial axially symmetric heating due to impacts for each diameter bin, (3) compute the axisymmetric cooling history for each diameter and expand to local Cartesian coordinates, (4) insert each impact's thermal history at the appropriate time at a random location into a 4D (x, y, z, t) Cartesian array representing the entire Earth surface, and (5) assess the subsurface habitability by summing the volumes of temperature intervals representing different microbial tolerances. Steps 1, 2, and 5 closely follow the methods of Abramov and colleagues; our different approach to the thermal history in Steps 3 and 4 makes minor assumptions of linearity that both significantly improve resolution and vastly decrease computing time.

2.1. Projectile size and time distribution

Our baseline impactor population (Case 1a) is a representative, single realization from a Monte Carlo simulation of the interplanetary planetesimal population hitting the Earth subsequent to the Moon-forming impact (Marchi et al., 2014). The time interval is 4.5 to 3.5 Ga, spanning the Hadean and early Archean. Impacts are discretized at 25 Myr intervals (multiple impacts are applied at each step). The total mass 7.0×10^{22} kg (density 2700 kg m^{-3}) is dominated by the two largest planetesimals, or embryos (diameters 1700 and 3500 km), that impact at 4.475 Ga (the first post-4.5 Ga time step); the remainder of the population contains 2.8×10^{21} kg and has a size–frequency distribution (SFD) roughly following an incremental power law with slope between -2 and -3, down to a minimum diameter of 15 km (Fig. 1). Note that the total projectile mass is ∼1% of Earth's mass, which is compatible with a "late veneer" of highly siderophile elements (see Walker, 2009, for a review). After the initial two large projectiles, the mass flux decreases with a 1/e time constant ∼120 Myr but includes a "sawtooth" LHB in which the impact rate peaks at ∼4.1 Ga. Impact velocities are 16 km s^{-1} prior to 4.15 Ga and 25 km s^{-1} afterward, representing planetesimal stirring due to planetary migration (Bottke et al., 2012; Morbidelli et al., 2012). We also consider an alternative (Case 1b) that eliminates the three largest projectiles and has a total mass 2.1×10^{21} kg.

We compare (Case 2a) to the SFD and time interval used by Abramov and Mojzsis (2009). Our implementation of their SFD includes projectiles >5 km in diameter and has a total mass 1.6×10^{21} kg (Fig. 1). The impacts occur at 20 km s^{-1} and are randomly distributed over an LHB interval of 100 Myr—note that this time interval models only the LHB and not the entire late accretion. Following Abramov and Mojzsis (2009), we also treat an alternative (Case 2b) with tenfold mass in each bin. This last scenario is arbitrary and intended to test the upper limits of the effects of bombardment on habitability.

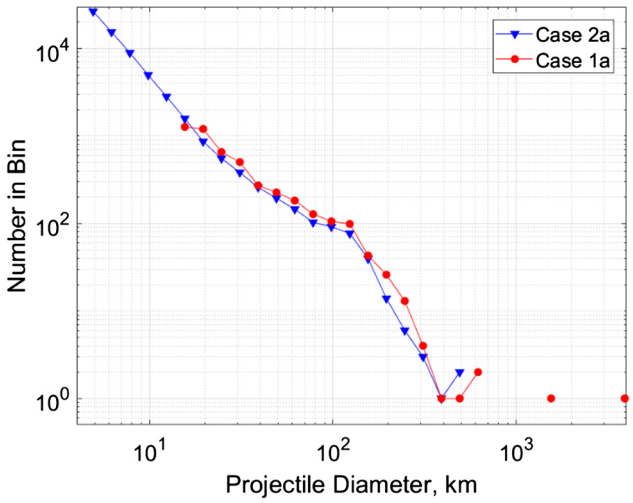

Fig. 1. Impactor size–frequency distributions (SFDs). Case 1a follows Marchi et al. (2014); Case 2a is rebinned from Abramov and Mojzsis (2009). Note two large remnant planetary embryos in Case 1a; the three largest projectiles are deleted in Case 1b. Case 2b uniformly scales Case 2a by 10×.

2.2. Impact heating

Subsurface heating due to impacts follows the detailed analytic treatment of Abramov et al. (2013), and Abramov and Mojzsis (2009), and we do not reproduce it here. The key steps are (1) calculation of a radial power law for peak shock pressure from impactor density, velocity, and impact angle, (2) conversion to waste heat using a Murnaghan equation of state, (3) structural uplift, and (4) topographic correction. Abramov et al. (2013) discussed validation of the predicted melt volumes against numerical models. We performed a rudimentary comparison of the heating predicted from the analytic model with a numerical model and found reasonable agreement (Appendix A).

The topographic correction involves shifting the isotherms at the transient crater elevation to the original horizontal surface and proportionately pulling up the isotherms below (Fig. 2). This is intended to reflect that heating length scales are large compared to topography so the latter can be conveniently considered flat. We derive slightly different results from Abramov et al. (2013) because they remove topography before applying structural uplift, whereas we do the reverse. Both are incorrect as sequences: future scaling should be done directly from hydrodynamic impact simulations and the final crater shape after the modification stage adopted for topographic correction. Here and in Abramov et al. (2013), the topographic correction sharply bends isotherms upwards below the former transient cavity: this defines the fundamental horizontal length scale as the transient cavity diameter D_{tc}.

2.3. Thermal evolution

For each projectile diameter (bin) d_p, the axially symmetric post-impact thermal anomaly $\Delta T(d_p, r_p, z_p)$ (where the subscript p indicates local, projectile coordinates) was expanded by Abramov and Mojzsis (2009) to Cartesian coordinates. Individual impacts were randomly placed into a 22 500-km square grid, with wrapping, representing the surface area of the Earth. Since depths affected by the impacts considered here are small compared to the planetary radius, the simpler Cartesian geometry can be efficiently used to track the overlapping thermal effects and to compute the integrals for habitable volumes. The model depth was 140 km, corresponding to a postulated lithospheric thickness. Transient 3D thermal conduction was simulated over this global grid (x, y, z) with the initial thermal disturbance of each impact added

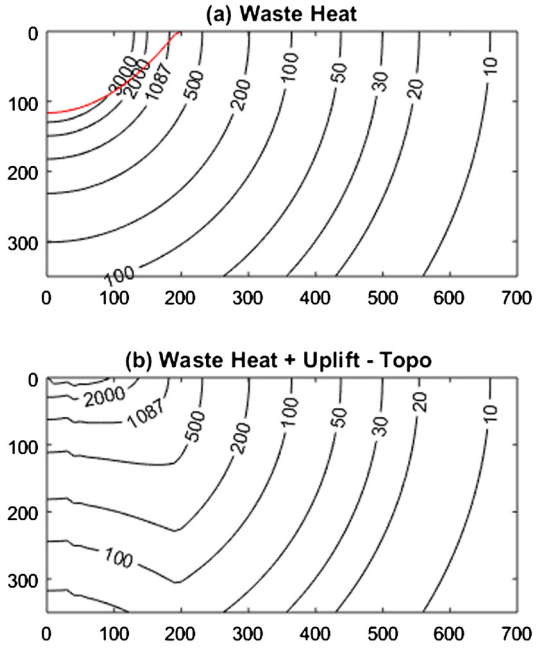

Fig. 2. Increase in subsurface temperatures ΔT (K) after impact (largely following Abramov and Mojzsis, 2009; Abramov et al., 2013) of a 100-km diameter projectile, 45° incidence, 20 km s^{-1}. (a) Initial ΔT from waste heat. Transient cavity is marked in red. (b) ΔT following topographic correction and structural uplift. Temperature anomaly is largely defined by diameter of former transient cavity.

at time t. Due to computational limitations, the grid spacing used by Abramov and co-workers was 300 km in x, y and 4.2 km in z. Because $D_{tc} = 300$ km for $d_p = 72$ km at $v = 20$ km s^{-1}, thermal anomalies are under-resolved for 97% of their projectile population (their minimum $d_p = 10$ km). Although this is only ~10% of the delivered energy, we argue in Appendix B that the area–time heating effect $\propto d_p^{0.46}$ for $d_p < 100$ km and $\propto d_p^{-0.54}$ for $d_p > 100$ km, which implies that >70% of the time-integrated temperature anomalies are under-resolved.

In order to resolve impact thermal anomalies for d_p larger than a few km, we adopted a mixed numerical-analytic *temporal linear superposition*. The complete thermal evolution for impacts of each projectile size $\Delta T(d_p, r_p, z_p, t_p)$ is calculated numerically in axisymmetry (using Comsol Multiphysics® 5.1) and translated to Cartesian coordinates. Where called for in the bombardment sequence, the 4D history for a particular d_p is added (analytically) into a 4D global grid (x, y, z, t). We specify only a limited number of depths in the global model, thus vastly saving memory. Our final global grid has resolution 30 km in x, y and 0.5 km in z, for the upper 10 km. Because $D_{tc} = 32$ km for $d_p = 4$ km at $v = 16$ km s^{-1}, the thermal anomalies produced by all projectiles in Fig. 1 are spatially resolved. The time resolution is automatically selected in the numerical model but is output at 25-Myr intervals for Case 1 and 2.5-Myr for Case 2, consistent with the temporal resolution of the impact-history models.

The analytic model for impact heating includes vapor and melt production. Vapor and excavated melt are removed from the model (large melt sheets are studied separately below). When the unexcavated melt cools in the numerical model, its latent heat is released over the liquidus–solidus temperature interval, 1200–1100 °C. These values follow Abramov et al. (2013); since pressure dependence of melting is neglected, we do not consider the effect of a background geotherm on melting either. Remelting of a partially cooled impact site by a subsequent impact neglects latent heat as such events are treated in the global 4D linear superposition. We will demonstrate that this effect is volumetrically minor. Even so, it has little effect on our study because energy is conserved and the influence on the low temperatures relevant to habitability is simply delayed.

Finally, we note that secondary impacts produce negligible heating relative to the primary population (Appendix C).

2.4. Boundary conditions and habitability model

The upper boundary of the axisymmetric thermal models is a constant 20 °C and the lower boundary is insulating, both for consistency with Abramov and Mojzsis (2009). A constant temperature or heat flux would be more appropriate to the bottom of the lithosphere, but the insulating condition provides a worst-case for habitability by maximizing temperatures. The conductive model formulated for the lithosphere implicitly assumes that deeper impact-induced thermal anomalies are mixed by mantle convection. The effects of different surface temperatures are discussed at the end of Section 3. The model radius is $7d_p$ so that the initial temperature perturbation is <10 K at the outer boundary.

Alternative gradients of 12 and 70 K/km (Abramov et al., 2013) are superimposed for the habitability assessment (another advantage of temporal linear superposition is that arbitrary background thermal structures can be added after the global model is completed). The latter represents a thinner, conductive lithosphere during the Hadean, whereas the former represents a locally (Korenaga, 2006) or globally (Moore and Webb, 2013) thicker lithosphere due to subduction zones or heat pipes, respectively.

Following Abramov and Mojzsis (2009), we adopt temperature habitability ranges for mesophiles, thermophiles, and hyperthermophiles of 20–50 °C, 50–80 °C, and 80–110 °C, respectively.

2.5. Melt sheets

We computed the resurfacing due melt sheets, assumed to apply only to $d_p \geq 100$ km (actually 94 km due to our binning) and having diameter $D_m = R_m d_p$, where $R_m = 20$–30 (Marchi et al., 2014). This is effectively repeating the work of Marchi and colleagues in our Cartesian geometry in order to compute the intervals between melt-sheet resurfacing. We separately investigated the thermal effects of melt sheets, also using Comsol 5.1. Assuming a constant melt-sheet thickness $h_m = 3$ km (Marchi et al., 2014), a 1D geometry can be evaluated because all $D_m \gg h_m$. The initial temperature of the melt sheet was 1400 °C, surface temperature 20 °C, latent heat was included, and the geothermal gradient alternately 12 and 70 K/km.

3. Results

Temperatures in the shallow subsurface at four times in the Case 1a bombardment are shown in Fig. 3. The large signatures of the two embryo impacts—essentially defining the end of accretion after the Moon-forming impact—are evident throughout much of the history. Sterile zones from impacts are always present but most of the area is quite close to the undisturbed surface temperature at any particular time.

Habitable volumes and their time evolution are quantified in Figs. 4 and 5, which differ by the assumed background temperature gradient. The equilibrium habitable volume for each microbe class compresses as the temperature gradient increases but the trends are the same for both geotherms. Fig. 6 shows the fraction of the top 1 km that is habitable by mesophiles, focusing on biomes that are most relevant to contemporary subsurface microbial life.

Habitable volumes increase nearly continuously for Case 1a, essentially in step with cooling as the bombardment wanes (there is a small bump in hyperthermophile habitability after the "sawtooth" at ~4.1 Ga). This behavior is dominated by the two embryo impacts, which sterilize most of the upper crust. The shallow

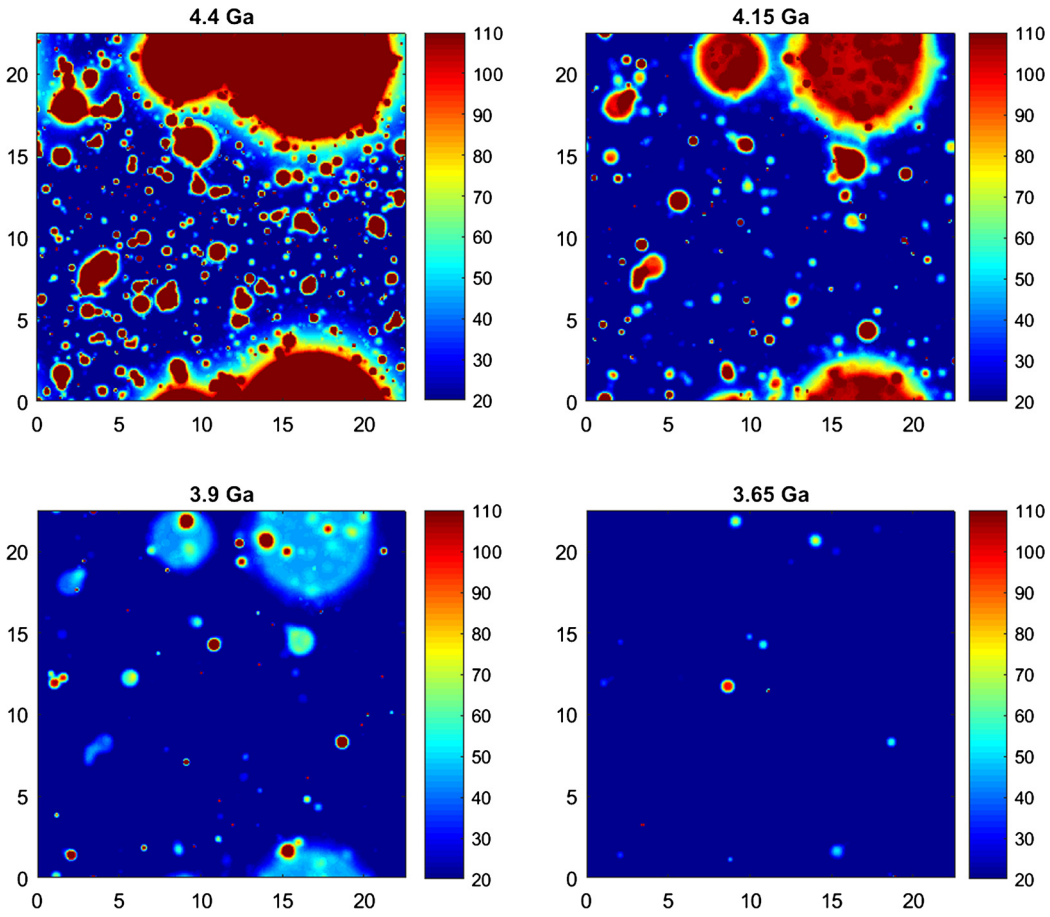

Fig. 3. Snapshots at 2-km depth for bombardment Case 1a. Note lasting effect of the two large embryo impacts. Temperature scale °C, axes are in 10^6 m.

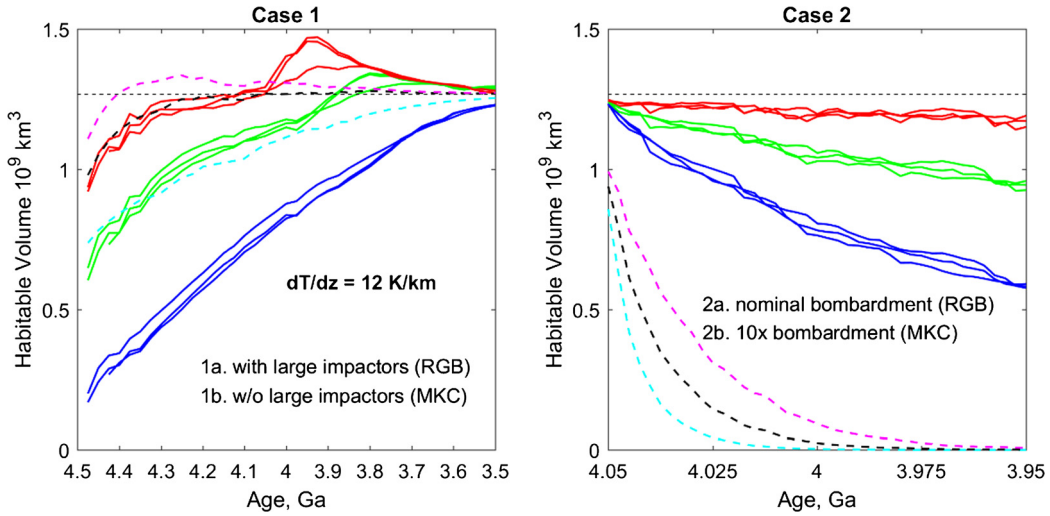

Fig. 4. Evolution of subsurface habitable volumes at 12 K/km geothermal gradient. *Left panel*: three geographical realizations of the Case 1a bombardment history include two large planetary embryos that impact at 4.475 Ga (RGB = red, green, blue curves). Single realization of Case 1b lacks these embryos (MKC = dashed magenta, black, and cyan curves). *Right panel*: Three geographical realizations of Case 2a bombardment history treat a discrete 100-Myr Late Heavy Bombardment (RGB curves). Case 2b (MKC dashed curves) applies ten times the number of projectiles in the same time interval. Curves are colored according to habitable temperature ranges for mesophiles (20–50 °C, blue and cyan), thermophiles (50–80 °C, green and black), and hyperthermophiles (80–110 °C, red and magenta). Because each microbe class is assigned a 30 K temperature interval, the habitable volumes are the same in the absence of bombardment (dotted black line). Habitable volumes under Case 1a, b grow nearly monotonically as bombardment wanes and impact heat dissipates. Shorter duration of LHB in Case 2a continuously decreases subsurface habitable volumes, but sterilization occurs only under extreme bombardment (Case 2b $\approx 8\times$ mass in 1/10 time as Case 1b).

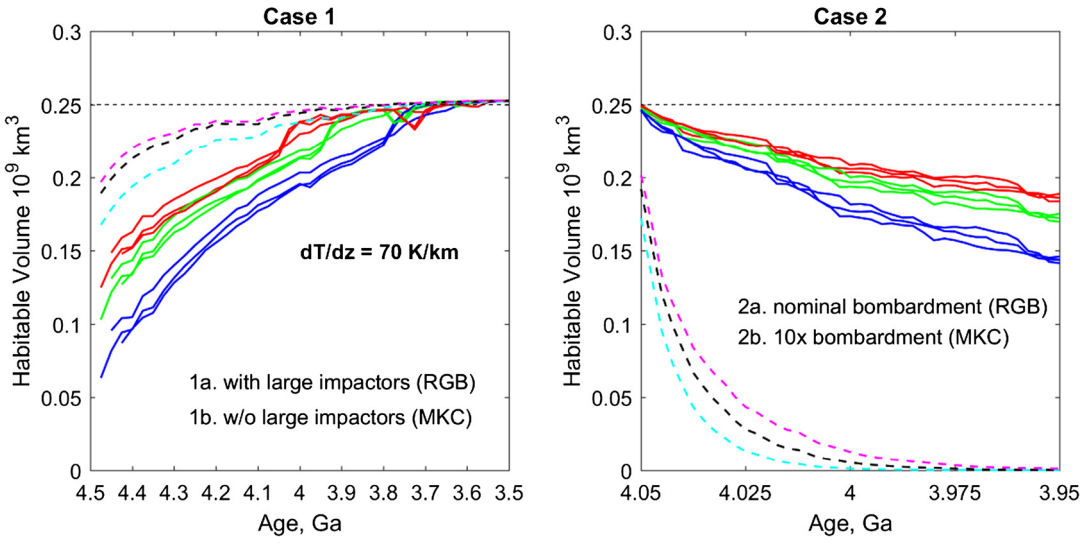

Fig. 5. Evolution of subsurface habitable volumes at 70 K/km geothermal gradient. Curves follow same scheme as Fig. 4. Although habitable zones are compressed compared to Fig. 4, the trends are similar.

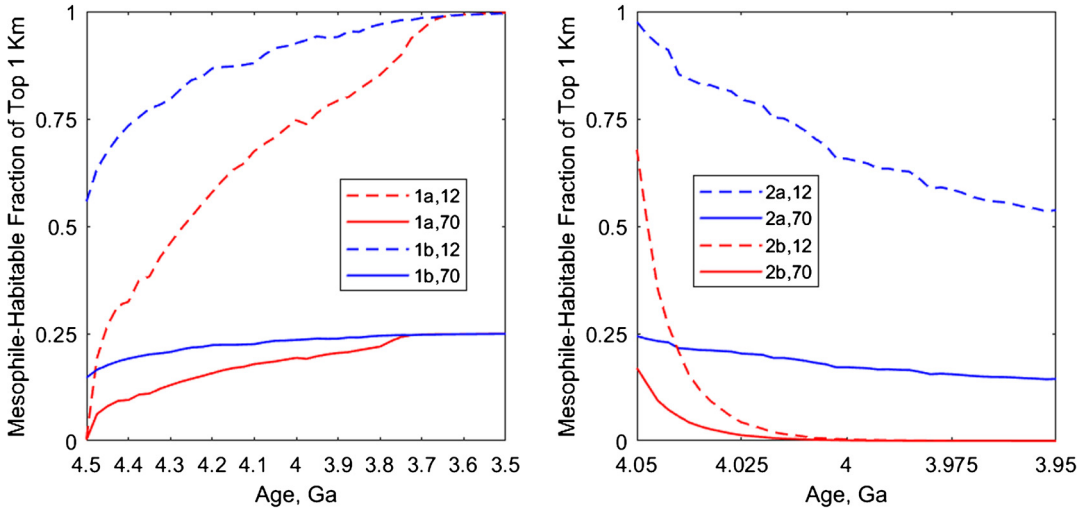

Fig. 6. Break-out of Figs. 4 and 5 showing fraction of uppermost kilometer that is habitable by mesophiles (maximum temperature 50 °C) as a function of time, each for a single model realization. Legend gives model scenario and geothermal gradient. Again note that Case 1 approaches with time the equilibrium habitable volume for each geotherm, whereas Case 2 decreases from the initial equilibrium states.

subsurface cannot be efficiently reheated because later impacts in Case 1a, while weighted to the Hadean, are nonetheless spread out over 1 Gyr. Case 1b, without the large embryos, approaches equilibrium more quickly.

In contrast, concentrating the early impact flux into a 100-Myr LHB (Case 2a) results in a continuous decrease in habitability because impact heat cannot dissipate during this short interval. In the extreme case of a tenfold increase in the number of impactors (Case 2b), the subsurface is completely, if transiently, sterilized. Note that this situations represents an 80× increase in the flux (mass/time) over Case 1b. A recent upward revision (Marchi et al., 2017) to the mass of the late impactor population by up to a factor of 2.5 over Case 1a still falls far short of the high fluxes demonstrated to cause sterilization.

While our Case 2a reproduces the bombardment history and impact heating of Abramov and colleagues, our calculations of habitable volume differ (compare to Fig. 4 in Abramov and Mojzsis, 2009; our color schemes are the same). They show only weak changes in habitable volume with time and the trends with respect to microbe class are also different. Furthermore, Abramov and Mojzsis (2009) stated that "even if all LHB impacts had occurred simultaneously, Earth still would not have been sterilized," whereas we find that the 10× multiplier to their projectile distribution would completely sterilize the subsurface. These discrepancies likely follow from under-resolution of their thermal-evolution calculations as described above.

We described above that the temporal linear superposition used to sum global thermal evolution of individual impacts does not treat latent heat when warm sites are heated above melting by a subsequent impact. We find that this situation occurs for <2% of the impact-summed upper 10 km of the crust in Cases 1a and 2a. Where the impactor flux is multiplied tenfold for Case 2b, ∼50% of the modeled volume experiences remelting. As described above, latent heat would delay changes at low temperature and so shift the habitable volume curves to the right (see Abramov et al., 2013 for related conclusions with regard to U–Pb age-resetting). Overall, 13% or less of the modeled volume was ever molten in Cases 1b and 2a, whereas the embryos in Case 1a push this fraction to ∼27%. Fully 77% of the upper 10 km melts in Case 2b.

The assumed surface temperature 20 °C does not account for possible variations introduced by changes in solar luminosity, planetary albedo, greenhouse gases, or other factors. A colder surface

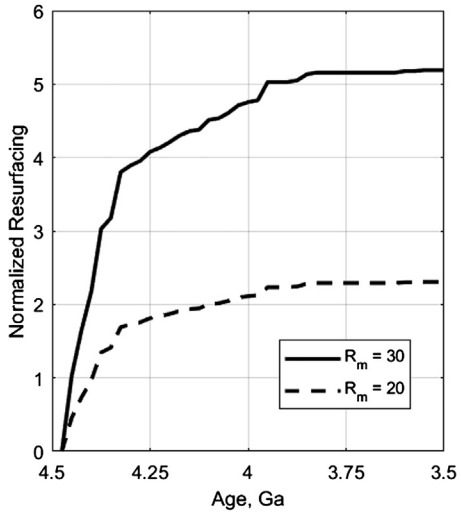

Fig. 7. Cumulative resurfacing by impact melt sheets for Case 1a, for two values of the ratio of melt sheet to projectile diameter R_m and applied to $d_p \geq 100$ km. Resurfacing in the first time bin at 4.475 Ga containing the largest projectiles has been subtracted. In the upper limit, the Earth is resurfaced several times over in the early Hadean, but cumulatively only once since ∼4.2 Ga.

would simply expand the habitable zones and reinforce our inference that it is difficult for bombardment to sterilize the subsurface. A warmer surface will compress the habitable zones. A surface temperature of 50 °C is straightforward to consider because it simply shifts thermophiles to the mesophile curves and extremophiles to the thermophile curves in Figs. 4 and 5, while eliminating all mesophile habitability. Similarly, Fig. 6 would then be relevant to thermophiles. Applied to organisms tolerant of higher temperatures, all of our prior conclusions hold.

We now turn to the effects of large melt sheets. The normalized cumulative resurfacing (Fig. 7) is the total area of all melt sheets produced over time, divided by the area of the Earth. The melt sheets from the two embryos in Case 1a are sufficient to resurface the Earth multiple times, so we subtract the resurfacing in this first time bin in Fig. 6. Even so, melt sheets produced by projectiles 100 km or larger cumulatively resurface the Earth several times during the Hadean. However, the waning bombardment results in just one cumulative (not simultaneous) resurfacing since ∼4.2 Ga at $R_m = 30$ and once since ∼4.35 Ga at $R_m = 20$.

Using geographically random realizations of the baseline Case 1a bombardment history, we find that the median age of the last melt-sheet burial and the median interval between burials are 4.1 Ga and 18 Myr, respectively, at $R_m = 30$. Examining only events older than 4 Ga, the median last burial and recurrence interval are 4.2 Ga and 12 Myr, respectively. Both of these values increase for $R_m = 20$; since we wish to compare the minimum recurrence time to a maximum cooling time, we will consider only $R_m = 30$.

The time–depth temperature histories for emplacement of a 3-km thick melt sheet were calculated for background geotherms of 12 and 70 K/km (Fig. 8). Recall that a 1D model is acceptable because thickness is much smaller than diameter. The habitable zones for the three classes of microbes start at equilibrium depths, are obliterated as heat from the melt sheet is conducted into the interior, and eventually are re-established at elevations 3 km higher. At 12 K/km, the time to 90% recovery of the equilibrium depths is 2.5 Myr, whereas at 70 K/km the 90% recovery time is just 0.5 Myr. The recovery is faster at higher geotherm because the equilibrium habitable zones are thinner. A characteristic thermal recovery time ∼1 Myr is an order of magnitude smaller than the worst-case melt-sheet recurrence interval of 12 Myr. This implies that biomes could be readily reestablished in the subsurface in between melt-sheet burials. In reality this would involve fracturing of the solidified melt sheet, infiltration of groundwater or the ocean, and transfer of organisms from other locations. Abramov et al. (2013) discuss faster cooling with hydrothermal circulation.

The median age of the last local melt-sheet emplacement 4.1–4.2 Ga, calculated here in wrapped Cartesian geometry, is consistent with the distribution of impact ages calculated under spherical geometry (Marchi et al., 2014) using the same bombardment history. The coincidence with Hadean zircon ages hints that impacts may have played an active role in zircon formation. Marchi et al. (2014) suggested that Hadean zircons may have formed below melt sheets in weathered country rocks that were heated to the inferred crystallization temperature ∼680 °C (Harrison, 2009). Here we find that contact heating is unlikely to provide such conditions deeper than a few hundred meters below the melt sheet (Fig. 7). Kenny et al. (2016) claimed that at least some Hadean zircons could have formed via direct crystallization from the melt, but this was challenged by Wielicki et al. (2016). Alternatively, impact-driven subduction could explain the coincidence between bombardment and zircon ages (O'Neill et al., 2017).

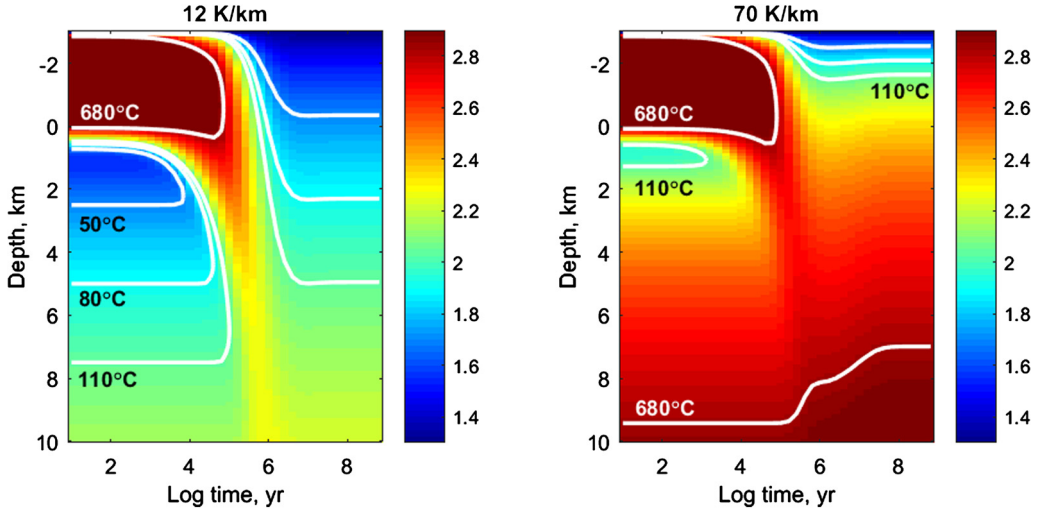

Fig. 8. Conductive temperature evolution within and below 3-km thick melt sheet emplaced at 1400 °C. Surface temperature is 20 °C. Color scale is log °C. Black contour labels are limits to habitable zones based on assumed temperature tolerance of different microbes (see text). Habitable zones recover to 90% of the equilibrium depths in ∼1 Myr. White contour label is mean crystallization temperature of Hadean zircons (Harrison, 2009) which, if related to melt sheets, can form only in the melt sheet itself and not by affecting country rock.

4. Concluding discussion

We modeled the Hadean and early Archean bombardment of the Earth using two projectile distributions: Case 1 includes several large projectiles, including two post-Moon-forming embryos >1000 km in diameter, but is distributed over 1 Gyr. Case 2 matches the Case 1 distribution at smaller diameters but is compressed into a 100-Myr Late Heavy Bombardment. An alternative to Case 1 neglects the large embryos, whereas an alternative to Case 2 increases the number of projectiles tenfold. We modeled the thermal evolution produced by the summed initial impact heating and subsequent cooling of every projectile, for geographically random realizations of each bombardment history. We find that the protracted bombardment of Case 1 results in a continuous increase with time in the total volume of subsurface habitable zones, because heating cannot keep up with the cooling of earlier impacts. In contrast, the shorter bombardment time for Case 2 results in net heating of the upper crust and a continuous decrease in habitable volume, although the crust is not completely sterilized until the projectile flux is arbitrarily increased tenfold.

The extensive melt sheets produced by the projectiles >100 km in diameter have recently been recognized to have widely buried and re-buried the Earth's surface during the Hadean bombardment (Marchi et al., 2014). However, we find that thermal recovery times are short (∼1 Myr) compared to recurrence intervals (>10 Myr), so biomes could be reestablished in between burials.

Our model extends previous work by Abramov and Mojzsis (2009) and Abramov et al. (2013) through more accurate thermal modeling and a revised assessment of Hadean and early Archean bombardment history. The computed temperature distributions are of course still idealized because they are static and do not account for other geologic processes. Crustal rebound, erosion, and uplift would enhance habitability by accelerating post-impact cooling. Lithospheric recycling will eliminate impact thermal anomalies in oceanic lithosphere on 100-Myr time scales but leave continental cratons and shields relatively untouched. This too represents a net improvement upon bombardment-imposed habitability. Volcanism would have an effect similar to impact-melt sheets, producing regional, short-lived sterilization. However, global volcanic burial rates of ∼1 mm/yr, appropriate to a heat-pipe early Earth (Moore and Webb, 2013), could continuously resterilize the subsurface.

We conclude that, for any reasonable bombardment scenario, the Hadean and early Archean were widely habitable in the subsurface. Future work can move away from consideration of direct impact heating by the complete size spectrum of projectiles and toward better modeling of surface, climate, and volcanotectonic effects due to large impactors, especially impact-driven global events like ocean vaporization or production of a silicate atmosphere from large impacts (Sleep and Zahnle, 1998).

Acknowledgements

Funding: This work was supported by the National Aeronautics and Space Administration, Exobiology grant number NNX15AL26G. We thank Steve Mojzis, an anonymous reviewer, and editor Bill McKinnon for constructive comments.

Appendix A. Comparison of analytical and numerical impact-heating models

In their previous study of the Hadean bombardment, Marchi et al. (2014) used the iSALE numerical model (Wünnemann et al., 2006) to compute impact-generated temperatures and melt volumes. As a simple test of the model used here (Abramov et al., 2013), we compared the depth at which both the analytic and numerical models produce a 1000-K temperature increase. The analytical model is evaluated on the original waste-heat deposition pattern (e.g., Fig. 2a). Results are in good agreement (Fig. A.1) but the isotherms predicted by the numerical model are consistently deeper than those of the analytical model. Scaling to the near-surface implies that the habitable zones resulting from individual impacts are proportionately increased for the numerical results. However, application over the SFD and consideration of the longevity of subsurface heating (Appendix B) indicates the discrepancy between the analytical and numerical models in the area–duration heating product is <15%, so refinement based on numerical modeling of impacts is deferred.

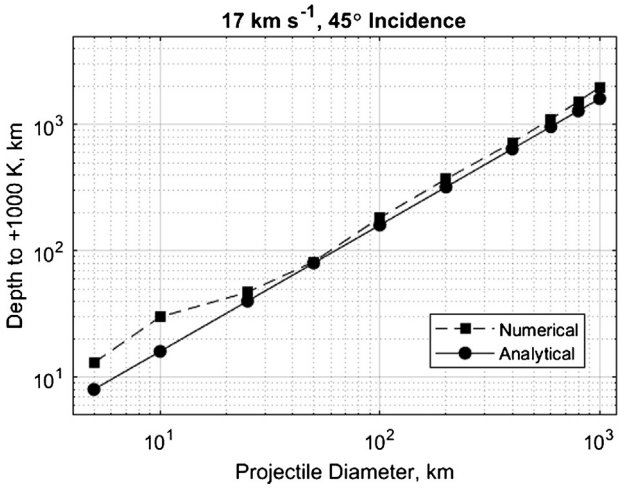

Fig. A.1. Comparison of depth to 1000 K temperature increase for analytical model used in this paper (Abramov et al., 2013) vs. iSALE numerical model (Wünnemann et al., 2006).

Appendix B. Effect of projectile diameter on time-integrated heating

We treated projectiles with $d_p > 15$ km in Case 1 and $d_p > 4.9$ km in Case 2. Abramov and Mojzsis (2009) discussed impactors as small as 1 km and claimed that sterilization (heating above 110 °C) for $d_p = 1$–10 km was as important as $d_p > 100$ km (note, however, that Abramov et al., 2013 state that only $d_p > 10$ km were used in the thermal evolution model). We argue that the integrated time-heating product is in fact maximized around $d_p = 100$ km. First, the SFD roughly follows $\propto d_p^{-2}$. Because the thermally affected area is approximately that of the transient cavity, $D_{tc}^2 \propto (d_p^{0.73})^2 = d_p^{1.46}$, so multiplying by the SFD implies that each d_p bin affects an area $\propto d_p^{-0.54}$. All 1–10 km objects are then seen to affect an area 3.5× bigger than 10–100 km. But the duration of heating t is shorter for smaller impacts and the balance will tip in favor of larger projectiles as long as $t \propto d_p^{0.54}$ or greater. Because the volume heated is approximately proportional to kinetic energy, the depth z to a particular isotherm is $z \propto d_p$. Now in simple diffusion, $t \propto z^2 \propto d_p^2$, far exceeding the tipping point. In practice, however, the near-surface, biologically relevant environment experiences $t \propto z \propto d_p$ due to the influence of the constant-temperature boundary condition. Therefore the net area–time heating product is $\propto d_p^1 d_p^{-0.54} = d_p^{0.46}$. This means the total area–time sterilization effect at 1–10 km is about 35% of that at 10–100 km. A non-negligible but non-critical fraction of the sterilization is lost by not treating the huge number of smaller impactors. At $d_p > 100$ km, however, the SFD slope is closer to −3, so the effect of larger projectiles is diminished as the area–duration heating product is now $\propto d_p^{-0.54}$. The effect of impact heating therefore is maximized at $d_p = 100$ km.

Appendix C. Energy in secondary impacts

A single impact can produce a multitude of secondary projectiles (e.g., McEwen and Bierhaus, 2006) that also heat the ground, potentially decreasing the habitable volumes considered in our model. We estimate the ratio of kinetic energy in the entire SFD of secondary projectiles compared to its primary as follows. The crater produced by the largest secondary projectile is ∼5% of the diameter of the primary crater (McEwen and Bierhaus, 2006). Using the scaling relations in Abramov and Mojzsis (2009), the diameter of the largest secondary projectile is $d_{s1} = 0.02 d_p (v_p / v_{s1})^{0.56}$, where d_p is the diameter of the primary, v_p is the impact velocity of the primary, and v_{s1} is the ejection velocity of the largest secondary. We specify 10^6 secondaries and, given the mass of the largest secondary, determine the slope b of the log–log cumulative SFD so that the total mass of secondaries = 1% of the primary (Vickery, 1987). The velocity v_s of an arbitrary secondary projectile with diameter d_s is taken as $v_s = v_{s1}(d_s/d_{s1})^{-1.9}$ (Vickery, 1987). Small secondaries exceeding escape velocity are eliminated. Taking $v_p = 20$ km s^{-1} and $v_{s1} = 1$–3 km s^{-1}, we find $b = -2.6$ to -3.5, reasonable for secondary projectile populations, and kinetic energy $\sim 10^{-4}$ of the primary population. The heating effects of secondary cratering, compared to the primary impact, are negligible.

Appendix D. Supplementary material

Supplementary material related to this article can be found online at https://doi.org/10.1016/j.epsl.2017.12.043.

References

Abramov, O., Mojzsis, S.J., 2009. Microbial habitability of the Hadean Earth during the late heavy bombardment. Nature 459, 419–422. https://doi.org/10.1038/nature08015.

Abramov, O., Kring, D.A., Mojzsis, S.J., 2013. The impact environment of the Hadean Earth. Chem. Erde 73, 227–248. https://doi.org/10.1016/j.chemer.2013.08.004.

Abramov, O., Mojzsis, S.J., 2016. Thermal effects of impact bombardments on Noachian Mars. Earth Planet. Sci. Lett. 442, 108–120.

Bottke, W.F., Walker, R.J., Day, J.M.D., Nesvorny, D., Elkins-Tanton, L., 2010. Stochastic late accretion to Earth, the Moon, and Mars. Science 330, 1527–1530. https://doi.org/10.1126/science.1196874.

Bottke, W.F., Vokrouhlický, D., Minton, D., Nesvorný, D., Morbidelli, A., Brasser, R., Simonson, B., Levison, H.F., 2012. An Archaean heavy bombardment from a destabilized extension of the asteroid belt. Nature 485, 78–81. https://doi.org/10.1038/nature10967.

Cloud, P., 1972. A working model of the primitive Earth. Am. J. Sci. 272, 537–548. https://doi.org/10.2475/ajs.272.6.537.

Harrison, T.M., 2009. The Hadean crust: evidence from >4 Ga zircons. Annu. Rev. Earth Planet. Sci. 37, 479–505. https://doi.org/10.1146/annurev.earth.031208.100151.

International Commission on Stratigraphy, 2017. http://www.stratigraphy.org/index.php/ics-chart-timescale.

Kenny, G.G., Whitehouse, M.J., Kamber, B.S., 2016. Differentiated impact melt sheets may be a potential source of Hadean detrital zircon. Geology 44, 435–438. https://doi.org/10.1130/G37898.1.

Korenaga, J., 2006. Archean geodynamics and the thermal evolution of Earth. In: Benn, K., Mareschal, J.-C., Condie, K.C. (Eds.), Archean Geodynamics and Environments. American Geophysical Union, pp. 7–32.

Kring, D.A., Cohen, B.A., 2002. Cataclysmic bombardment throughout the inner solar system 3.9–4.0 Ga. J. Geophys. Res. 107. https://doi.org/10.1029/2001JE001529.

Marchi, S., Bottke, W.F., Elkins-Tanton, L.T., Bierhaus, M., Wuennemann, K., Morbidelli, A., Kring, D.A., 2014. Widespread mixing and burial of Earth's Hadean crust by asteroid impacts. Nature 511, 578–582. https://doi.org/10.1038/nature13539.

Marchi, S., Canup, R.M., Walker, R.J., 2017. Heterogeneous delivery of silicate and metal to the Earth by large planetesimals. Nat. Geosci. 1. https://doi.org/10.1038/s41561-017-0022-3.

McEwen, A.S., Bierhaus, E.B., 2006. The importance of secondary cratering to age constraints on planetary surfaces. Annu. Rev. Earth Planet. Sci. 34, 535–567. https://doi.org/10.1146/annurev.earth.34.031405.125018n.

Mojzsis, S.J., Harrison, T.M., Pidgeon, R.T., 2001. Oxygen-isotope evidence from ancient zircons for liquid water at the Earth's surface 4,300 Myr ago. Nature 409 (6817), 178–181. https://doi.org/10.1038/35051557.

Moore, W.B., Webb, A.G., 2013. Heat-pipe Earth. Nature 501, 501–505.

Morbidelli, A., Marchi, S., Bottke, W.F., Kring, D.A., 2012. A sawtooth-like timeline for the first billion years of lunar bombardment. Earth Planet. Sci. Lett. 355, 144–151. https://doi.org/10.1016/j.epsl.2012.07.037.

O'Neill, C., Debaille, V., 2014. The evolution of Hadean–Eoarchean geodynamics. Earth Planet. Sci. Lett. 406, 49–58. https://doi.org/10.1016/j.epsl.2014.08.034.

O'Neill, C., Marchi, S., Zhang, S., Bottke, W., 2017. Impact-driven subduction on the Hadean Earth. Nat. Geosci. 10, ngeo3029. https://doi.org/10.1038/ngeo3029.

Ryder, G., 2002. Mass flux in the ancient Earth–Moon system and benign implications for the origin of life on Earth. J. Geophys. Res. 107. https://doi.org/10.1029/2001JE001583.

Sleep, N.H., Zahnle, K., 1998. Refugia from asteroid impacts on early Mars and the early Earth. J. Geophys. Res. 103, 28529–28544. https://doi.org/10.1029/98JE01809.

Vickery, A.M., 1987. Variation in ejecta size with ejection velocity. Geophys. Res. Lett. 14, 726–729. https://doi.org/10.1029/GL014i007p00726.

Walker, R.J., 2009. Highly siderophile elements in the Earth, Moon and Mars: update and implications for planetary accretion and differentiation. Chem. Erde 69, 101–125. https://doi.org/10.1016/j.chemer.2008.10.001.

Wielicki, M.M., Harrison, T.M., Schmitt, A.K., Boehnke, P., Bell, E.A., 2016. Differentiated impact melt sheets may be a potential source of Hadean detrital zircon: comment. Geology 44, e398. https://doi.org/10.1130/G38135C.1.

Wilde, S.A., Valley, J.W., Peck, W.H., Graham, C.M., 2001. Evidence from detrital zircons for the existence of continental crust and oceans on the Earth 4.4 Gyr ago. Nature 409, 175–178.

Wünnemann, K., Collins, G.S., Melosh, H.J., 2006. A strain-based porosity model for use in hydrocode simulations of impacts and implications for transient crater growth in porous targets. Icarus 180, 514–527. https://doi.org/10.1016/j.icarus.2005.10.013.